1-1-2013

Experimental study of optimal energy weighting in energy-resolved CT using a CZT detector

Franco Rupcich
Marquette University, franco.rupcich@marquette.edu

Taly Gilat-Schmidt
Marquette University, tal.gilat-schmidt@marquette.edu

PROCEEDINGS OF SPIE

Experimental study of optimal energy weighting in energy-resolved CT using a CZT detector

Franco Rupcich, Taly Gilat-Schmidt

SPIE.

Experimental study of optimal energy weighting in energy-resolved CT using a CZT detector

Franco Rupcich[a] and Taly Gilat Schmidt[a]

[a]Department of Biomedical Engineering, Marquette University, Milwaukee, WI, USA;

ABSTRACT

Recent advances in energy-resolved CT can potentially improve contrast-to-noise ratio (CNR), which could subsequently reduce dose in conventional and dedicated breast CT. Two methods have been proposed for optimal energy weighting: weighting the energy-bin data prior to log normalization (projection-based weighting) and weighting the energy-bin data after log normalization (image-based weighting). Previous studies suggested that optimal projection-based and image-based energy weighting provide similar CNR improvements for energy-resolved CT compared to photon-counting or conventional energy-integrating CT. This study experimentally investigated the improvement in CNR of projection-based and image-based weighted images relative to photon-counting for six different energy-bin combinations using a bench top system with a CZT detector. The results showed CNR values ranged between 0.85 and 1.01 for the projection-based weighted images and between 0.91 and 1.43 for the image-based weighted images, relative to the CNR for the photon-counting image. The range of CNR values demonstrates the effects of energy-bin selection on CNR for a particular energy weighting scheme. The non-ideal spectral response of the CZT detector caused spectral tailing, which appears to generally reduce the CNR for the projection-based weighted images. Image-based weighting increased CNR in five of the six bin combinations despite the non-ideal spectral effects.

Keywords: CT dose reduction, energy-resolved CT, dedicated breast CT, multi-energy CT, energy-weighted CT, cadmium zinc telluride, breast imaging

1. INTRODUCTION

In recent years, dedicated breast CT has received attention as a viable breast imaging modality,[1–7] due to its expected lower costs than MRI, higher sensitivity than mammography, and lack of compression. One early study demonstrated the potential for obtaining high signal-to-noise ratio (SNR) images using dedicated breast CT at dose levels comparable to those used in mammography.[1] In addition, recent advances in photon-counting detector technology have motivated investigations[4–6] of the ability of energy-resolved CT to produce high-contrast diagnostic images, which could subsequently lead to reduced breast dose.

Because the contrast between biological tissues is generally greater at lower energies, an ideal detector is one that would assign more weight to lower-energy photons. Thus, conventional energy-integrating detectors, which assign more weight to higher-energy photons, and photon-counting detectors, which assign equal weights to all photons, are sub-optimal. Energy-resolving CT detectors, on the other hand, are capable of sorting photons into discrete energy bins based on specified energy thresholds. This additional spectral information can then be used to produce optimally energy-weighted images.

Previous work has suggested that optimal energy weighting provides increased contrast-to-noise ratio (CNR) for energy-resolved CT compared to photon-counting and conventional energy-integrating CT,[4–6,8,9] which suggests the potential for reduced dose during conventional and dedicated breast CT. This study experimentally investigated the effects of energy-bin selection on the improvement in CNR of projection-based and image-based weighted images relative to photon counting during energy-resolved CT. Further, we performed a preliminary investigation of the effects of spectral tailing on the performance of image-based and projection-based weighting, where spectral tailing is the non-ideal detector spectral response that causes high energy photons to be detected in lower energy bins.[10] Our long term goal is to quantify the potential for image quality improvement and/or dose reduction for energy-resolved breast CT.

2. METHODS AND MATERIALS

2.1 Overview

We acquired multi-energy CT data of a breast phantom containing a calcium contrast agent using our bench top energy-resolving CT system with a cadmium zinc telluride (CZT) detector. Images were obtained using both projection-based and image-based weighting for six different energy-bin combinations, and the CNR for each energy-bin combination for both weighting schemes was compared to that of an image obtained using photon-counting detection.

2.2 Bench top energy-resolving CT system

Our bench top energy-resolving CT system (Figure 1a) consists of a cadmium zinc telluride (CZT) detector (NEXIS, Nova R&D, Riverside, CA) with two pixel rows, each consisting of 128, 1×1 mm pixels. The detector pixel array is read out by the XENA chip (Nova R&D, Riverside, CA), which can sort detected photons above user-selected energy thresholds into a maximum of five bins per acquisition. The system also consists of a microfocal x-ray source (Fein-Focus-100.50, YXLON Intl, Hamburg, Germany) with a 3 micron effective focal spot. Cylindrical phantoms can be affixed to a rotating stage positioned between the x-ray source and CZT detector.
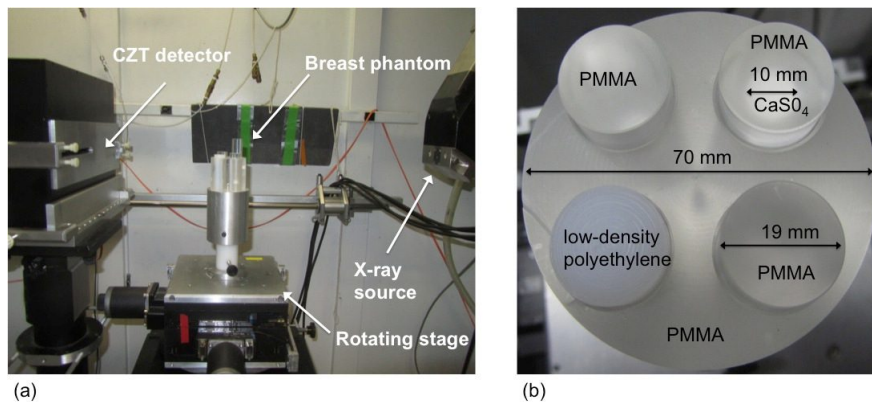

Figure 1. (a) Bench-top system and (b) breast phantom.

2.3 Breast phantom

A phantom representing the breast was constructed from a 70-mm diameter PMMA cylinder containing four, 19-mm-diameter cylindrical inserts composed of the following materials: 1) PMMA embedded with a 10 mm diameter calcium sulfate element, 2) low-density polyethylene (representing adipose tissue), 3) and 4) PMMA (Figure 1b).

2.4 System calibration

The detector energy-bin threshold settings were calibrated by sweeping the threshold levels while acquiring transmission measurements through channels containing iodine solution and tungsten film. The k-edges of iodine and tungsten were identified from the transmission measurements and used as reference threshold settings.

Knowledge of the x-ray spectrum is required for calculating the optimal projection-based weights and for investigating the spectral tailing effects. The x-ray spectrum was estimated from transmission measurements through varying thicknesses of acrylic and Teflon. The spectrum was estimated using measurements of all counts above the lowest energy threshold (i.e, photon counting detection), and was therefore unaffected by spectral tailing. An expectation maximization algorithm[11] estimated the spectrum that maximized the likelihood of obtaining the transmission measurements.

2.5 Acquiring projections

Two hundred projections of the phantom were acquired in step-and-shoot mode over 360° (1.8° per projection) at 100 kV and 8.8 mAs. Flat-field projections were collected at 100 kV and 4.4 mAs. The source-to-detector distance was 72 cm, and the source-to-isocenter distance was 40 cm. The raw photon count for each projection was measured using eight detector energy threshold bins: 25, 30, 35, 40, 45, 50, 60, and 70 keV. The total photon count between any two energy thresholds was obtained by calculating the difference in counts between those two threshold bins. Six combinations of energy bins (Table 1) were constructed from the raw data.

Table 1. Energy-bin combinations investigated for projection-based and image-based weighting

Bin Combination	Energy-bin Cutoff (keV)							
	1	2	3	4	5	6	7	8
1	25-30	30-35	35-40	40-45	45-50	50-60	60-70	>70
2	25-35	35-45	>45	-	-	-	-	-
3	25-35	35-50	>50	-	-	-	-	-
4	25-40	40-60	>60	-	-	-	-	-
5	25-30	30-35	35-40	40-50	50-60	60-70	>70	-
6	25-40	40-50	50-60	60-70	>70	-	-	-

2.6 Weighting and reconstructing images

For each energy-bin combination in Table 1, projections were flat-field corrected and images were obtained using projection-based and image-based weighting. In addition, we reconstructed a reference photon-counting image. All images were reconstructed with filtered backprojection. Details on the implementation of each weighting scheme are provided in the following subsections.

2.6.1 Photon-counting

A photon-counting detector weights each photon equally, independent of its energy. Therefore, the raw projections obtained from the lowest energy threshold (all photons with an energy above 25 keV) were log-normalized and reconstructed to obtain a photon-counting image.

2.6.2 Projection-based weighting

Projection-based optimal energy weighting linearly combines the energy-bin data prior to log normalization, with the weights proportional to the expected contrast-to-noise-variance ratios (CNVRs) of the binned projection data.[5,12] The optimal energy-dependent weights for maximizing CNR between a projection through background material and a projection through background material with an embedded contrast element of length d are described in Equation 1:[13,14]

$$w_{PB}(E) = \frac{1 - e^{-[\mu_c(E) - \mu_b(E)]d}}{1 + e^{-[\mu_c(E) - \mu_b(E)]d}} \tag{1}$$

where μ_b and μ_c are the energy-dependent linear attenuation coefficients of the background and contrast element materials, respectively. For each bin combination, we estimated the projection-based line integrals by weighting, combining, and then log-normalizing the projection data according to Equation 2:[5]

$$\tilde{\ell}_{PB} = -\ln\left(\frac{\sum_{i=1}^{M}(w_{PBi} \cdot \int_{E_i} N_0(E)e^{-\int \mu(l,E)dl}dE)}{\sum_{i=1}^{M} w_{PBi} \cdot \int_{E_i} N_0(E)dE}\right) \tag{2}$$

where M is the number of energy bins, E_i is the energy range of the ith bin, $N_0(E)$ is the number of incident photons at each energy, E, and $\mu(l,E)$ is the energy-dependent linear attenuation coefficient of the object along ray path, l. The weight of the ith bin, w_{PBi}, was estimated using Equation 1 assuming the average attenuation coefficients, $\bar{\mu}_i$ as described in Equation 3:

$$\bar{\mu}_i = \int_{E_i} \mu(E) \cdot \Phi(E)dE \tag{3}$$

where $\Phi(E)$ is the estimated normalized spectrum, as described in Section 2.4. Once the projection data were weighted, combined, and log-normalized, we used filtered backprojection reconstruction to obtain a projection-based weighted image for each energy-bin combination described in Table 1.

2.6.3 Image-based weighting

Whereas projection-based weighting performs a linear combination of the energy-binned data prior to log normalization and reconstruction, image-based weighting performs a linear combination of the reconstructed energy-bin images:[5]

$$Image_{combined} = \sum_{i=1}^{M} w_{IBi} \cdot Image_i \qquad (4)$$

The optimal weights are derived to maximize the CNR in the final reconstructed image. The optimal weight of the ith energy-bin image, w_{IBi}, is proportional to the CNVR of the binned images, and is calculated using Equation 5:[5]

$$w_{IBi} = \frac{C_i/\sigma_i^2}{\sum_{n=1}^{M} C_n/\sigma_n^2} \qquad (5)$$

where σ_i is the noise standard deviation and C_i the contrast in the ith energy-bin image. Image-based weights may also be calculated prior to reconstructing the energy-bin images.[5] Assuming the use of a linear reconstruction algorithm, such as filtered back projection, we can obtain an image equivalent to that described by Equation 4 by weighting and combining the energy-bin data after log-normalization but before reconstruction. This method requires only a single reconstruction of the combined energy-bin data, and the estimated image-based weighted line integral is:[5]

$$\tilde{\ell}_{IB} = \sum_{i=1}^{M} -w_{IBi} \ln \left(\frac{\int_{E_i} N_0(E) e^{-\int \mu(l,E)dl} dE}{\int_{E_i} N_0(E) dE} \right) \qquad (6)$$

We performed image-based weighting using the first method – linearly combining the reconstructed energy-bin images, as described in Equation 4. We estimated the contrast using the following equation:

$$C_i = |\bar{\mu}_{c,i} - \bar{\mu}_{b,i}| \qquad (7)$$

where $\bar{\mu}_{c,i}$ and $\bar{\mu}_{b,i}$ are the mean reconstructed attenuation coefficients within regions-of-interest (ROIs) of the calcium contrast element and background material, respectively, in the ith energy-bin image. Similarly, σ_i was estimated as the standard deviation within a background ROI in the ith enegy-bin image. Two reconstructed images for each energy bin were subtracted from one another to obtain an estimate of the standard deviation in images containing only noise, thus preventing ring artifacts from contributing to the noise estimate. Similarly, the background and calcium ROIs were circular regions with equivalent diameters and at an equivalent radius from the phantom center, thereby assuring the same relative effects of ring artifacts on the means of both ROIs.

2.7 Assessment of image quality

For each energy-bin combination, we measured the contrast, noise, and CNR for the projection-based and image-based weighted images relative to the photon-counting image. Contrast was estimated as the absolute value of the difference between the means of a background ROI and an ROI within the calcium element. Noise was estimated as the standard deviation of a background ROI. For all cases, two reconstructions were performed and the images subtracted to obtain a noise-only image and prevent ring artifacts from contributing to the noise estimate, as described in Section 2.6.3. Similarly, contrast and background ROIs were chosen carefully so that any ring artifacts would have the same effect on the means of both ROIs, also described in Section 2.6.3.

3. RESULTS

Figure 2 shows the individual energy-binned images for bin combination 5. In general, the lower energy bins demonstrate higher contrast and noise, while the higher energy bins demonstrate the opposite.

Table 2 lists the contrast, noise, and CNR for each energy-bin combination for projection-based and image-based weighting relative to those of the photon-counting image. The ratios of the CNR of the energy-weighted images over the photon-counting image ranged between 0.85 (bin combinations 1 and 4) and 1.01 (bin combination 3) for the projection-based weighted images and between 0.91 (bin combination 2) and 1.43 (bin combination 5) for the image-based weighted images. In general, the projection-based weighted images showed relatively
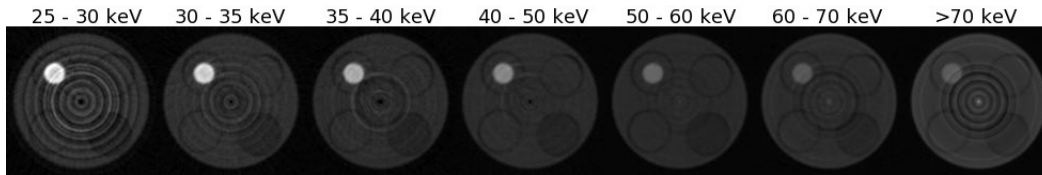

Figure 2. Individual energy-binned images for bin combination 5. All images are shown at the same window (7800 HU) and level (2700 HU).

higher contrast at the expense of higher noise, resulting in lower CNR compared to the photon counting case for all but one of the six bin combinations. While the image-based weighted images demonstrated relatively lower contrast, they also produced lower noise, resulting in higher CNR than the photon counting case for five of the six bin combinations. These results are visually evident in Figure 3, which displays images reconstructed using projection-based and image-based weighting for energy-bin combinations 3 and 5, along with the photon-counting image.

Table 2. Results for projection-based and image-based weighted images. Contrast, noise, and CNR are reported relative to the photon-counting case.

	Projection-Based Weighting				Image-Based Weighting		
Bin Combination	Contrast	Noise (stdev)	CNR	Bin Combination	Contrast	Noise (stdev)	CNR
1	1.11	1.30	0.85	1	0.82	0.79	1.04
2	0.94	1.06	0.89	2	0.79	0.87	0.91
3	1.01	1.00	1.01	3	0.80	0.67	1.20
4	1.15	1.35	0.85	4	0.92	0.69	1.33
5	1.10	1.18	0.93	5	0.85	0.59	1.43
6	1.01	1.06	0.95	6	0.75	0.65	1.15

Figure 4a plots the CNR for each bin combination for projection-based and image-based weighting relative to photon-counting. The differences in the shape of the curves suggests that an optimal bin combination (in terms of CNR) depends on the type of weighting used. Figure 4b plots the normalized photon-counting, projection-based, and image-based weights for bin combination 5. For this particular bin combination, the projection-based weighting gives more weight to the lower energy photons, whereas the image-based weighting gives more weight to the higher energy photons.

In theory, both image-based and projection-based weighting should provide CNR that is at least as good as photon-counting weighting. As seen in Table 2, the CNR was equal to or lower than the photon-counting CNR for all projection-based weighted images and for one image-based weighted image. This discrepancy is likely caused by the fact that the theoretically calculated weights in the case of projection-based weighting may not reflect the measured CNVR in the energy-bin projection data. To quantify the magnitude of spectral tailing in the measured data, Figure 5 plots the number of photons expected at each energy bin based on the estimated 100 kV spectrum (whose measurement was minimally affected by spectral tailing, as described in Section 2.4) and the number of photons measured in each bin of a flat-field projection. The lowest two energy bins detected nearly 4.5 and 2.5 times the number of expected photons, respectively, while the highest three energy bins detected
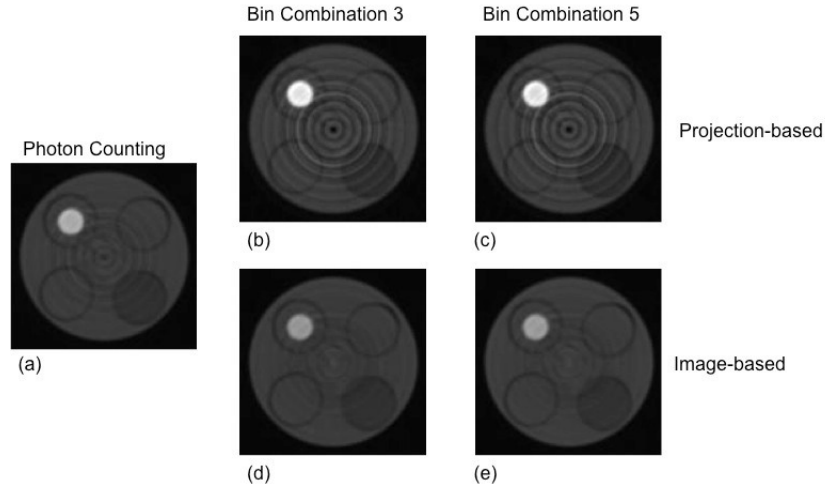
Figure 3. Images reconstructed using (a) photon-counting; (b) projection-based weighting with bin combination 3; (c) projection-based weighting with bin combination 5; (d) image-based weighting with bin combination 3; (e) image-based weighting with bin combination 5. All images have the same window (6000 HU) and level (1800 HU).
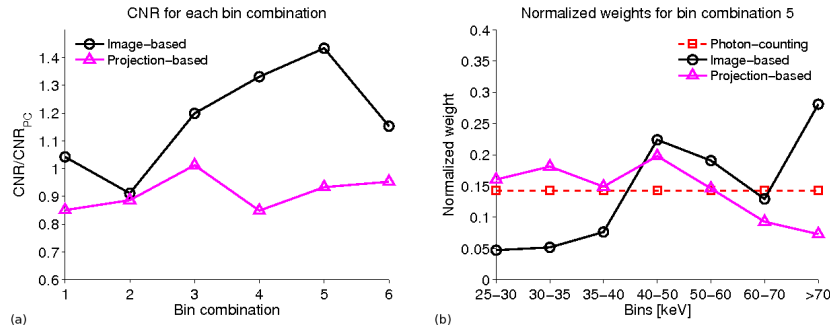

Figure 4. (a) CNR for each bin combination of projection-based and image-based weighting, relative to photon-counting. (b) Normalized photon-counting, image-based, and projection-based weights for bin combination 5.

between 0.5 and 0.83 the number of expected photons, indicating the presence of spectral tailing. Due to the presence of more higher energy photons, spectral tailing reduces the contrast in the lower energy bins. On the other hand, the increase in the total number of photons in the bin leads to a reduction in noise. The inverse is true for the higher energy bins.
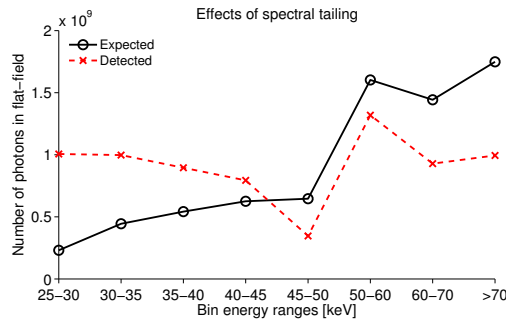

Figure 5. The number of detected photons in the flat-field projection for each energy bin and the number of expected photons in each energy bin for the estimated 100 kV spectrum

4. DISCUSSION AND CONCLUSIONS

Previous work suggested similar CNR performance for optimal projection- and image-based weights.[5,6] Furthermore, previous work also predicted that optimal weighting improves contrast compared to photon-counting weighting, due to the increased weighting of the low-energy bins.[4–6,8] In our preliminary experimental results, projection-based weighting provided reduced CNR compared to photon-counting, and the images resulting from image-based weighting had increased CNR but reduced contrast compared to photon counting. We believe these discrepancies are due to the non-ideal spectral response in the CZT detector, which leads to spectral tailing effects, i.e., higher energy photons being counted in lower energy bins (Figure 5). Results suggest that these spectral tailing effects generally reduce the CNR in images reconstructed with projection-based weighting. On the other hand, image-based weighting was able to produce improved CNR despite the spectral tailing effects. This is likely due to the fact that the projection-based weights estimated in this work were based on the theoretical task, while the image-based weights were estimated from the measured image data (i.e., noise and contrast estimated directly from the binned images). Thus, the image-based weights may be adjusted to at least partially account for such system non-idealities. The results of the projection-based weighting could be improved by calculating the weights based on estimates of contrast and noise obtained directly from the projection data, although this measurement may be challenging in practice. The reduced ring artifacts in the image-based weighted images are likely caused by the increased weighting of high-energy bins, due to spectral tailing, compared to the projection-based weights. Work is in progress to develop methods to correct the spectral tailing response[6,10,15–18] to provide further CNR improvements for energy weighting with energy-resolving detectors.

Overall, our results indicate that image-based weighting during energy-resolved CT improves CNR and thus shows potential for reducing breast dose during procedures such as dedicated breast CT. Further studies are required to investigate the performance of each weighting scheme when combined with spectral tailing correction.

ACKNOWLEDGMENTS

REFERENCES

[1] Boone, J. M., Nelson, T. R., Lindfors, K. K., and Seibert, J. A., "Dedicated breast CT: radiation dose and image quality evaluation," *Radiology* **221**, 657–667 (2001).

[2] McKinley, R. L., Tornai, M. P., Samei, E., and Bradshaw, M. L., "Simulation study of a quasi-monochromatic beam for x-ray computed mammotomography," *Medical Physics* **31**, 800–813 (2004).

[3] Glick, S. J., Thacker, S., Gong, X., and Liu, B., "Evaluating the impact of x-ray spectral shape on image quality in flat-panel CT breast imaging," *Medical Physics* **34**, 5–24 (2007).

[4] Shikhaliev, P. M., "Energy-resolved computed tomography: first experimental results," *Physics in Medicine and Biology* **53**(20), 5595–5613 (2008).

[5] Schmidt, T. G., "Optimal image-based weighting for energy-resolved CT," *Medical Physics* **36**(7), 3018–3027 (2009).

[6] Kalluri, K., Glick, S. J., and Mahd, M., "SNR Improvement in Dedicated Breast CT using Energy Weighting with Photon Counting Detectors," in [*2011 37th Annual Northeast Bioengineering Conference (NEBEC)*], *IEEE*, 1–2 (2011).

[7] Shikhaliev, P. M. and Fritz, S. G., "Photon counting spectral CT versus conventional CT: comparative evaluation for breast imaging application," *Physics in Medicine and Biology* **56**, 1905–1930 (2011).

[8] Le, H. Q., Ducote, J. L., and Molloi, S., "Radiation dose reduction using a CdZnTe-based computed tomography system: Comparison to flat-panel detectors," *Medical Physics* **37**(3), 1225–1236 (2010).

[9] Shikhaliev, P. M., "The upper limits of the SNR in radiography and CT with polyenergetic x-rays," *Physics in Medicine and Biology* **55**(18), 5317–5339 (2010).

[10] Schlomka, J. P., Roessl, E., Dorscheid, R., Dill, S., Martens, G., Istel, T., Bäumer, C., Herrmann, C., Steadman, R., Zeitler, G., Livne, A., and Proksa, R., "Experimental feasibility of multi-energy photon-counting K-edge imaging in pre-clinical computed tomography.," *Physics in Medicine and Biology* **53**(15), 4031–4047 (2008).

[11] Sidky, E. Y., Yu, L., Pan, X., Zou, Y., and Vannier, M., "A robust method of x-ray source spectrum estimation from transmission measurements: Demonstrated on computer simulated, scatter-free transmission data," *Journal of Applied Physics* **97**(12), 124701–124701–11 (2005).

[12] Giersch, J., Niederlöhner, D., and Anton, G., "The influence of energy weighting on X-ray imaging quality," *Nuclear Instruments and Methods in Physics Research A* **531**(1-2), 68–74 (2004).

[13] Tapiovaara, M. and Wagner, R. F., "SNR and DQE analysis of broad spectrum X-ray imaging," *Physics in Medicine and Biology* **30**(6), 519–529 (1985).

[14] Shikhaliev, P. M., "Computed tomography with energy-resolved detection: a feasibility study," *Physics in Medicine and Biology* **53**(5), 1475–1495 (2008).

[15] Ding, H. and Molloi, S., "Image-based spectral distortion correction for photon-counting x-ray detectors," *Medical physics* **39**(4), 1864 (2012).

[16] Schmidt, T. G., "An empirical method for correcting the detector spectral response in energy-resolved CT," in [*Medical Imaging 2012: Physics of Medical Imaging*], Pelc, N. J., Nishikawa, R. M., and Whiting, B. R., eds., *Proceedings of SPIE* **8313**, 831312–1–831312–6 (2012).

[17] Srivastava, S., Cammin, J., Fung, G. S. K., Tsui, B. M. W., and Taguchi, K., "Spectral response compensation for photon-counting clinical x-ray CT using sinogram restoration," in [*Medical Imaging 2012: Physics of Medical Imaging*], Pelc, N. J., Nishikawa, R. M., and Whiting, B. R., eds., *Proceedings of SPIE* **8313**, 831311–1 – 831311–7 (2012).

[18] Wang, X., Meier, D., Mikkelsen, S., Maehlum, G. E., Wagenaar, D. J., Tsui, B. M. W., Patt, B. E., and Frey, E. C., "MicroCT with energy-resolved photon-counting detectors," *Physics in Medicine and Biology* **56**(9), 2791–2816 (2011).